



Seismic Retrofit of Structures Using Hybrid Steel Slit–Viscoelastic Dampers

Mohammad Seddiq Eskandari Nasab¹ and Jinkoo Kim²

Abstract: A hybrid steel slit–viscoelastic damper (HSVD) has been developed to enhance seismic performance of a structure. To model viscoelastic behavior, an analytical model is developed based on the Kelvin–Voigt and Bouc–Wen–Baber–Noori (BWBN) models. Experimental studies are conducted to find out the behavior of the viscoelastic material and the hybrid damper, and to validate the analytical model. Various seismic performance indices are evaluated using a three-story moment-resisting frame before and after seismic retrofit with the steel slit dampers and HSVDs. Fragility analysis is then carried out to investigate the exceedance probability of specified limit states, which shows that adding a viscoelastic part to the steel slit damper successfully improves the performance of the steel slit dampers. Finally, it is observed that the use of the capacity and demand diagram procedure is effective in preliminary design of the hybrid dampers to meet a desired target performance goal. DOI: [10.1061/\(ASCE\)ST.1943-541X.0002816](https://doi.org/10.1061/(ASCE)ST.1943-541X.0002816). © 2020 American Society of Civil Engineers.

Author keywords: Seismic retrofit; Viscoelastic dampers; Slit dampers; Fragility analysis; Damping devices.

Introduction

To protect structures and their residents from earthquakes, many energy dissipation devices have been investigated (Chan and Albermani 2008; Xu et al. 2016; Lee and Kim 2017; Javidan and Kim 2019, 2020). Passive energy dissipation devices are generally reliable and sometimes cost-effective compared with traditional seismic retrofit techniques such as jacketing of structural members, installation of shear walls or steel braces, and so on. Passive energy dissipation devices can be categorized as velocity-dependent or displacement-dependent devices according to their mechanical behavior [FEMA 273 (FEMA 1997)].

Recently, considerable efforts have been made to maximize energy dissipation capability by introducing various combinations of passive devices. For instance, Tsai et al. (1998) and Uetani et al. (2003) investigated the combined effects of passive devices to overcome limitations of velocity-dependent or displacement-dependent dampers. Kasai et al. (2002) developed a viscoelasto–plastic damper combining velocity-dependent and displacement-dependent devices in series. Test results validated superior performance of the hybrid damper as compared to a single device. Marko et al. (2004) studied the combined friction–viscoelastic damping devices, strategically placed inside of shear walls, and assessed the impact of its damping on the structures. Marshall and Charney (2012) had analytically examined four combinations of a buckling restrained brace and either a viscoelastic or viscous fluid device in a series arrangement. They showed that any arrangement improved some part of structural responses for common and severe seismic events. Lee and Kim (2015)

studied the efficiency of a hybrid damper composed of steel slit plate and rotational friction devices to be effectively used in major and minor earthquakes. Montgomery and Christopoulos (2015) developed a new damping system by adding high damping elements in place of reinforced concrete coupling beams to enhance the wind and seismic performance of coupled shear-wall high-rise buildings. Lee et al. (2016) and Nour Eldin et al. (2018) proposed a hybrid damper consisting of steel strip and friction dampers. To this end, quasi-cyclic experiments were conducted on 10 specimens. The results showed that the friction-strip dampers are stable and effective in resisting seismic loads as expected. Guo and Christopoulos (2016) developed hybrid passive damping devices that combine the advantage of viscoelastic and friction damping, and proposed a design method based on the performance spectra framework for systems equipped with hybrid dampers. Kim and Shin (2017) carried out cyclic loading tests and seismic loss assessment of a structure retrofitted with steel slit linear friction hybrid dampers developed for seismic retrofit of existing structures. The results showed that the linear friction–slit dampers are stable and effective in resisting seismic loads as expected. Pant et al. (2017) developed a method using viscoelastic dampers as coupling members between reinforced concrete shear walls that has been recently developed for enhancing the wind performance and seismic resilience of tall buildings. Naem et al. (2017) examined the seismic performance of a framed structure retrofitted using steel slit dampers combined with shape memory alloy bars. They showed that the hybrid damper is effective in reducing both maximum and residual displacements caused by earthquake ground motions. Naem and Kim (2018a, b) developed an analysis model and carried out a shaking table test of a two-story steel frame retrofitted with a self-centering viscous damper combined with a pre-stressed tendon. In the field of seismic retrofit of bridge structures, Xiang and Alam (2019) carried out a comparative seismic fragility assessment of an existing isolated continuous bridge retrofitted with different energy dissipation devices, and found that shape-memory alloy cable is the most effective in mitigating the seismic vulnerability of the bridge system at all the damage states.

In this study, a hybrid steel slit–viscoelastic damper (HSVD) is developed by a combining steel slit damper with a viscoelastic damper to enhance the energy dissipation capability of conventional steel slit dampers. By combining displacement-dependent

¹Research Assistant, Dept. of Civil and Architectural Engineering, Sungkyunkwan Univ., Suwon 16419, Republic of Korea. ORCID: <https://orcid.org/0000-0002-0607-1024>. Email: eskandari@skku.edu

²Professor, Dept. of Civil and Architectural Engineering, Sungkyunkwan Univ., Suwon 16419, Republic of Korea (corresponding author). ORCID: <https://orcid.org/0000-0002-3605-8189>. Email: jkim12@skku.edu

Note. This manuscript was submitted on May 30, 2019; approved on June 3, 2020; published online on August 21, 2020. Discussion period open until January 21, 2021; separate discussions must be submitted for individual papers. This paper is part of the *Journal of Structural Engineering*, © ASCE, ISSN 0733-9445.

and velocity-dependent devices, it is intended that the hybrid dampers can be effective both in small and large earthquakes with only slight increase in material and manufacturing costs. During minor earthquakes, the slit plate remains elastic and only the viscoelastic part works to dissipate seismic energy; and for major earthquakes, both the viscoelastic and steel slit parts work simultaneously to dissipate large seismic energy. It can also be expected that the dampers are useful for decreasing both displacement and velocity in structures induced by earthquakes. Figs. 1(a and b) shows the overall view and components of the HSVD. The damper is designed to be small in size, especially in thickness, by arranging the two individual dampers side by side. This is advantageous when HSVD is placed inside of a partition wall.

To characterize the material properties of the viscoelastic damper, 42 tests are conducted with different frequencies and amplitudes on the two viscoelastic specimens. Based on the experimental results on viscoelastic material, the Bouc–Wen–Baber–Noori (BWBN) model is developed in the context of the Kelvin–Voigt model. In addition, a cyclic loading test is conducted on the HSVD to assess its seismic energy dissipating capacity and to validate the analysis model. A three-story moment-resisting frame is then chosen from the SAC Phase II project, and the developed analysis model is used to assess the contribution of the viscoelastic part in improving seismic performance of the retrofitted structure. To this end, various seismic performance indices of the model structure are evaluated before and after seismic retrofit with the slit damper and HSVDs. Fragility analysis is then carried out to investigate the exceedance probability of specified limit states. Finally, a performance-based design procedure is applied to a four-story steel frame to estimate the required amount of the hybrid dampers to meet a desired target performance goal.

Tests of Viscoelastic Dampers

Test Specimens and Setup

The viscoelastic pad is made of high-damping rubber, which has the following chemical composition: natural rubber (26.0%), synthetic rubber (13.0%), liquid rubber (13.0%), carbon black (40.1%), antioxidant (3.9%), zinc oxide (2.6%), accelerator (0.6%), and sulfur (0.3%). Fig. 2(a) shows the components of a single viscoelastic damper, which are two high-damping rubber pads and three steel plates. Two viscoelastic damper specimens are fabricated [Fig. 2(b)] and displacement-controlled cyclic loading is applied along the longitudinal axis of the dampers. The dampers

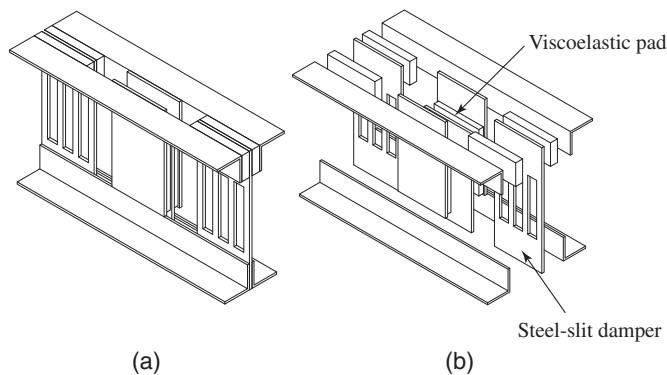


Fig. 1. Configuration of the HSVD: (a) hybrid damper; and (b) components of the damper.

consist of two layers of $225 \times 175 \times 18$ mm viscoelastic material bonded in between three steel plates. The viscoelastic damper is made to be much smaller than the commercially available viscoelastic dampers used for seismic retrofit of building structures in consideration of the capacity of the fatigue testing machine used; however, it is expected to be enough to enhance the performance of the slit damper. Fig. 2(c) shows the MTS testing machine (MTS Systems Corporation) with the capacity of 250 kN and the installation of the dampers.

Viscoelastic Material Test Protocols

To obtain the material properties of the viscoelastic pads, 42 harmonic displacement-controlled tests with different frequencies and amplitudes are carried out on the two viscoelastic damper specimens. The frequencies used in these tests are 0.05, 0.2, and 0.5 Hz. Seven amplitudes are considered in these tests in which the first amplitude is 1.8 mm and the other amplitudes are calculated by Eq. (1)

$$a_n = 2(n-1)a_1 \quad (1)$$

where a_1 and n = first amplitude and number of steps, respectively.

Analysis Model

Viscoelastic solid materials exhibit both elastic solid and Newtonian liquid characteristics during deformation. The conventional viscoelastic constitutive models, Maxwell and Kelvin–Voigt models, consist of the spring and dashpot, which are representatives of ideal elastic solid and ideal Newtonian liquid characteristics, respectively. The Kelvin–Voigt model is composed of elastic stiffness, K_{ve} , and viscous damping, C_{ve} connected in parallel, and the produced force at a given circular frequency by the viscoelastic material can be calculated as the sum of restoring force, F_R , and damping force, F_D

$$F_{VE} = F_D + F_R = C_{ve}\dot{u} + K_{ve}u \quad (2)$$

where u = viscoelastic relative shear displacement at time t . In this model, it is assumed that the restoring force is elastic and there is no hysteretic component. The stiffness and the damping of a viscoelastic damper are represented as follows using the storage modulus G' , loss modulus G'' , and loss factor η

$$\eta = \frac{G''}{G'} \quad (3)$$

$$K_{ve} = \frac{G'A_b}{t} \quad C_{ve} = \frac{G''A_b}{\omega t} \quad (4)$$

where A_b and t = bonded area and the total thickness of the viscoelastic material pad; and ω = natural frequency of the model structure.

For a linear elastic system, the Kelvin–Voigt model is generally accepted to represent the behavior of a viscoelastic damper. However, under strong earthquakes, responses of structure and the damper may exceed the elastic range. In addition, Xue (2013) showed that the Kelvin–Voigt model has large deviation in representing the behavior of viscoelastic solid material. Thus, in this study, an analytical model is developed by combining the Kelvin–Voigt model and the nonlinear BWBN model to more precisely simulate the behavior of the viscoelastic material. The derivation procedure of the BWBN model is summarized as follows (Foliente 1995; Hossain and Ashraf 2012; Xue 2013).

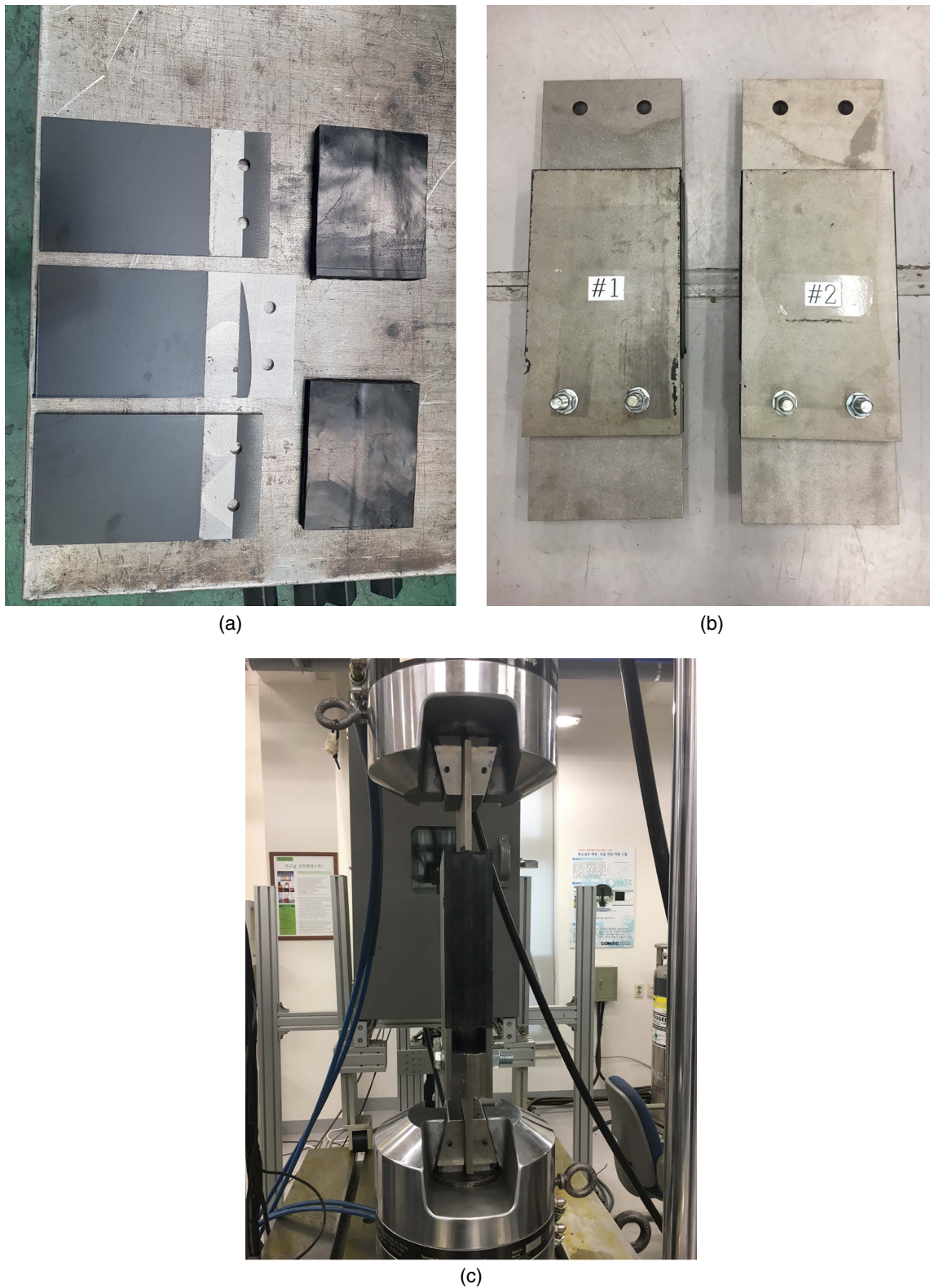


Fig. 2. Test of viscoelastic damper: (a) components of the damper; (b) test specimens; and (c) test setup.

The equation of a nonlinear system motion, which is assumed a single degree of freedom (SDOF) oscillator, can be expressed as

$$F_I + F_D + F_R = f(t) \quad (5)$$

where F_I = the inertia force; F_D = damping force; and F_R = restoring force, which is expressed as

$$F_R = F_e + F_h = \alpha k_0 \gamma + (1 - \alpha) k_0 z \quad (6)$$

where the elastic and hysteretic components of the restoring force F_R are represented by F_e and F_h , respectively. The parameter of α is the ratio of final tangent stiffness k_t to the initial stiffness k_0 , u is the relative of the mass, and z is the hysteretic

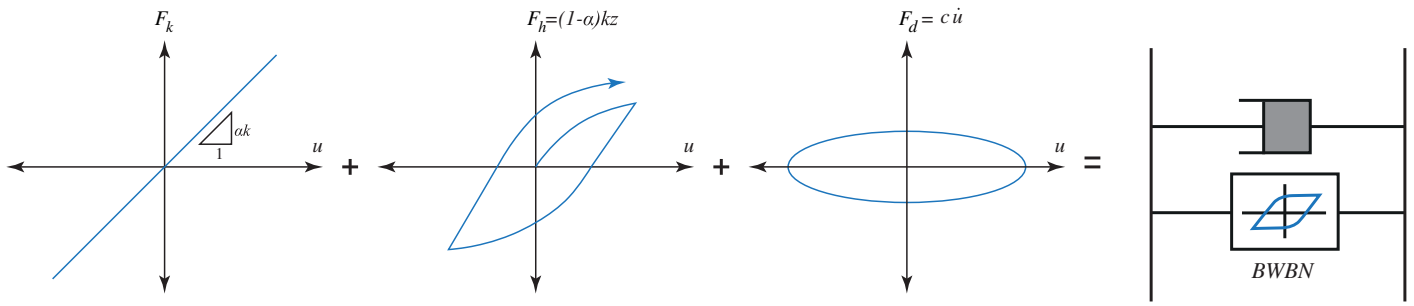


Fig. 3. BWN model for viscoelastic dampers.

displacement, which is calculated by the first-order nonlinear differential equation

$$\dot{z} = A\dot{u} - [\gamma\dot{u}|z|^n + \beta|\dot{u}||z|^{n-1}z] \quad (7)$$

where A, β, γ , and n = parameters controlling the shape of the hysteretic curve. To include the effect of residual force, Foliente (1995) suggested a pinching function shown in Eq. (9) multiplied to Eq. (7)

$$\dot{z} = h(z)(A\dot{u} - [\gamma\dot{u}|z|^n + \beta|\dot{u}||z|^{n-1}z]) \quad (8)$$

$$h(z) = 1.0 - \zeta_1 e^{\left(\frac{(z - \text{sgn}(\dot{u}) - qz_u)^2}{\zeta_2}\right)} \quad (9)$$

where z_u = ultimate value of z , which can be expressed as Eq. (10). The severity of the pinching can be controlled by ζ_1 which is limited to 0 or 1, while the spreading of the pinching region is defined by ζ_2 . Eqs. (11) and (12) define ζ_1 and ζ_2 as functions of hysteretic energy ε

$$z_u = \left[\frac{1}{\beta + \gamma}\right]^{\frac{1}{n}} \quad (10)$$

$$\zeta_1 = \zeta_{10}[1.0 - e^{(-p\varepsilon)}] \quad (11)$$

$$\zeta_2 = (\psi_0 + \delta_\psi\varepsilon)(\lambda + \zeta_1) \quad (12)$$

where the rate of initial drop is controlled by p , while δ_ψ controls the spreading of the pinching. The amount of pinching is affected by ψ_0 , and the changing rate of ζ_1 and ζ_2 is limited by λ . The changing rate of hysteretic energy ε is defined as follows:

$$\dot{\varepsilon} = (1 - \alpha)k_0z\dot{u} \quad (13)$$

In this study, the nonlinear behavior of the viscoelastic damper is realized by substituting the BWN model to the linear spring of Kelvin–Voigt model. Thus, as shown in Fig. 3, the produced force by the proposed model is the sum of the elastic restoring force, the hysteretic restoring force, and the viscous force. The damping coefficient is calculated similar to the Kelvin–Voigt model as given in Eq. (4), and the initial stiffness can be defined by initial storage modulus G'_0 as shown in Eq. (14)

$$k_0 = \frac{G'_0 A_b}{t} \quad (14)$$

Mechanical properties of the viscoelastic material are determined using both Kelvin–Voigt model and BWN model in the context of Kelvin–Voigt model. The storage modulus, loss factor, and the initial storage modulus are calculated based on the 42 tests and are shown in Fig. 4. To estimate the parameters of the BWN

model based on the test results, the nonlinear least-squares optimization method proposed by Hossain and Ashraf (2012) is used.

Comparison of Analysis and Test Results

The comparison of the analysis and test results of specimen No. 1 is presented in Figs. 5(a–h), in which the tests are carried out in two frequencies [Fig. 5(f)] of 0.05 and 0.5 Hz and two amplitudes [Fig. 5(d)] of 7.2 and 21.6 mm. Figs. 5(a–h) show that the modified BWN model can represent the behavior of the viscoelastic damper with more accuracy compared with the Kelvin–Voigt model, especially in the specimen subjected to larger displacement. Based on this observation, the modified BWN model, in which the linear spring of the Kelvin–Voigt model is replaced with the BWN model, is adopted to simulate the behavior of the viscoelastic material in the hybrid damper.

Hybrid Steel Slit–Viscoelastic Dampers

Modeling of Steel Slit Dampers

The HSVD investigated in this study is comprised of a viscoelastic damper and two steel slit dampers connected in parallel. The two slit dampers have a total of eight strips: the width (b), thickness (t), and the height (L_o) of each strip are 20, 9, and 200 mm, respectively. The in-plane stiffness of each steel slit damper subjected to horizontal shear force can be obtained as follows based on the assumption that the ends of the narrow strips are fully restrained from rotation

$$k_d = n \frac{12EI}{l_0^3} = n \frac{Etb^3}{l_0^3} \quad (15)$$

where n, t, b , and l_0 = number of strips, thickness of strips, width of strips, and length of the vertical strips, respectively. Chan and Albermani (2008) derived the yield strength of a slit damper assuming elastic–perfectly-plastic behavior, which is summarized as follows. Plastic hinges form at both ends of the strip with the full plastic moment, M_p , obtained by multiplication of the yield stress, σ_y , and the plastic section modulus

$$M_p = \sigma_y \frac{tb^2}{4} \quad (16)$$

From the equivalence of the internal work, $P_y\delta_p$, and the external work, $2nM_p\theta_p$, where δ_p is the plastic displacement and θ_p is the plastic rotation, the yield force of the slit damper, P_y , can be obtained as follows:

$$P_y = F_{y,slit} = \frac{2nM_p}{l_0} = \frac{n\sigma_y t b^2}{2l_0} \quad (17)$$

Description of Test Results and Analysis Modeling

Cyclic loading test of the HSVD is performed to understand the behavior of the damper including the shape of the hysteresis curve. Fig. 6(a) shows the dimensions of the HSVD test specimen, and Figs. 6(b–d) depict the test setup for the cyclic loading test. Cyclic load is applied horizontally using a servo actuator with the

maximum load capacity of 1,500 kN and maximum displacement of 400 mm. The transverse movement of the specimen during the test is prevented by a restrainer attached above the specimen. The loading protocol used in the test is prepared following the guidelines of FEMA 461 (FEMA 2007) as shown in Fig. 7(a). The minimum displacement imposed on the damper specimen is determined to be 1.98 mm, which corresponds to the yield point of the slit damper. After each two cycles of loading, the displacement amplitude is increased to 1.4 times the previous one until the displacement reaches the target displacement of 80 mm, which corresponds to 2.7% of the story height. It was observed that at the second step

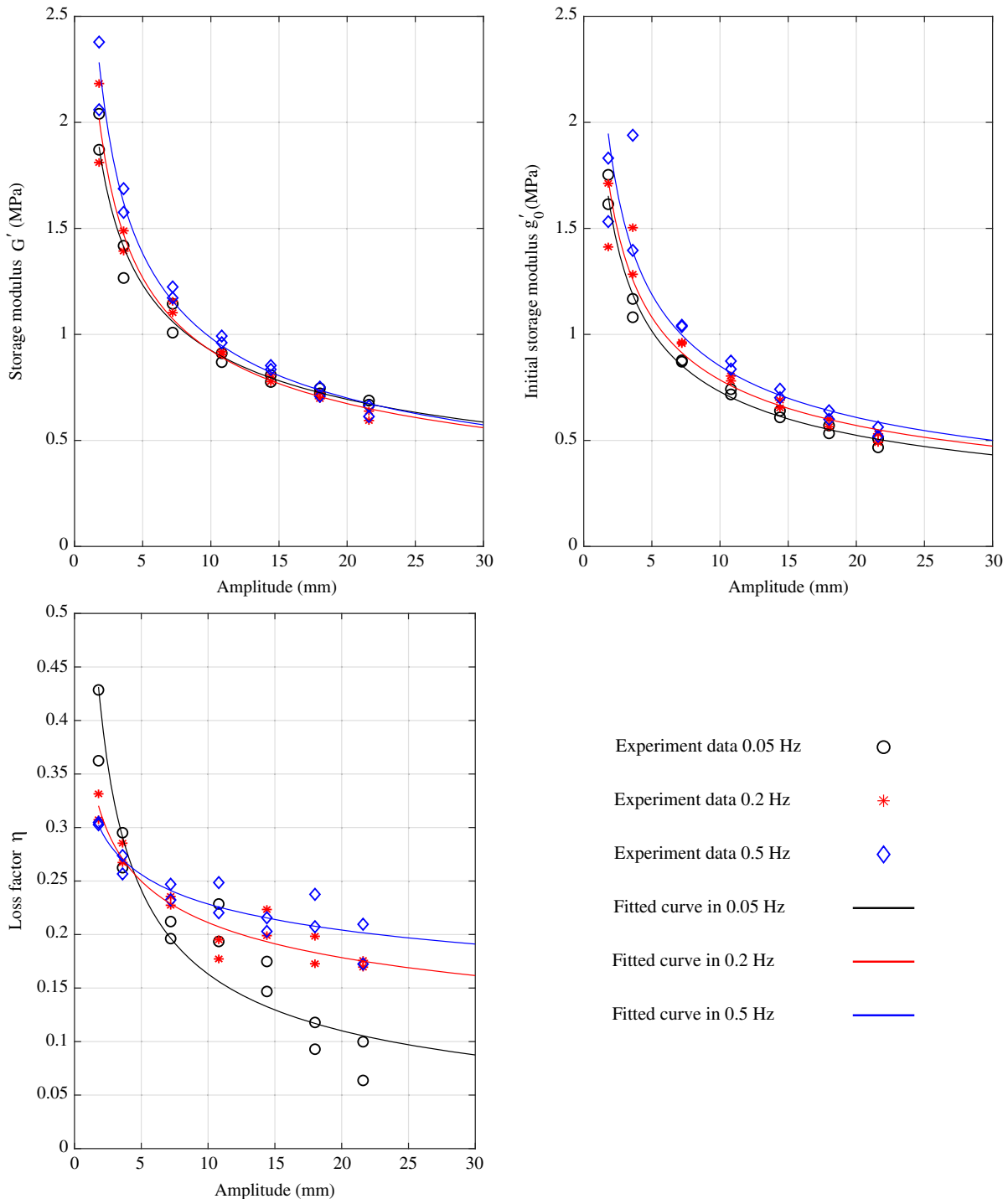


Fig. 4. Storage modulus and loss factor obtained from the tests.

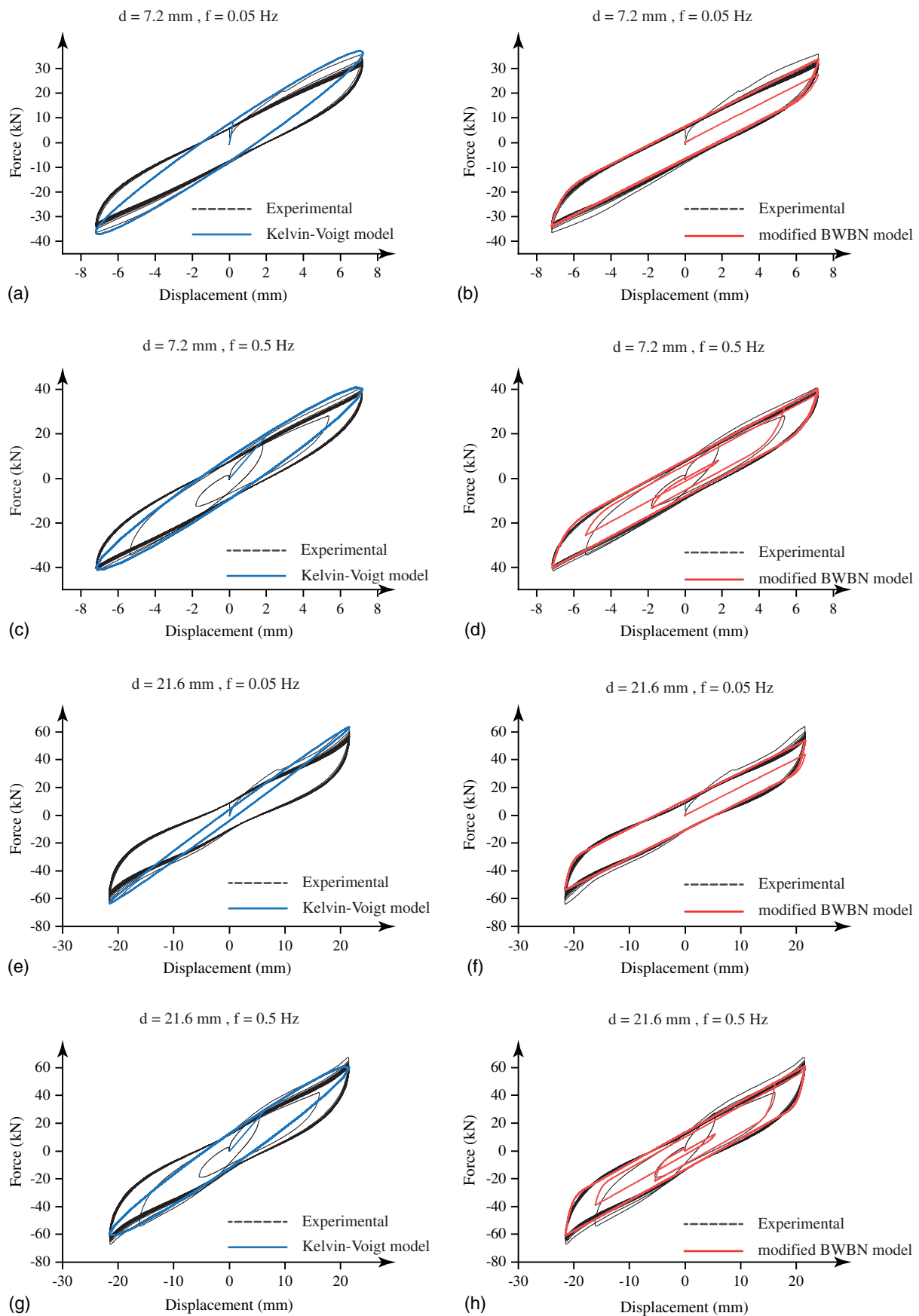


Fig. 5. Comparison of the test and simulation results of the viscoelastic damper: (a) Kelvin–Voigt ($d = 7.2$ mm, $f = 0.05$ Hz); (b) BWBN ($d = 7.2$ mm, $f = 0.05$ Hz); (c) Kelvin–Voigt ($d = 7.2$ mm, $f = 0.5$ Hz); (d) BWBN ($d = 7.2$ mm, $f = 0.5$ Hz); (e) Kelvin–Voigt ($d = 21.6$ mm, $f = 0.05$ Hz); (f) BWBN ($d = 21.6$ mm, $f = 0.05$ Hz); (g) Kelvin–Voigt ($d = 21.6$ mm, $f = 0.5$ Hz); and (h) BWBN ($d = 21.6$ mm, $f = 0.5$ Hz).

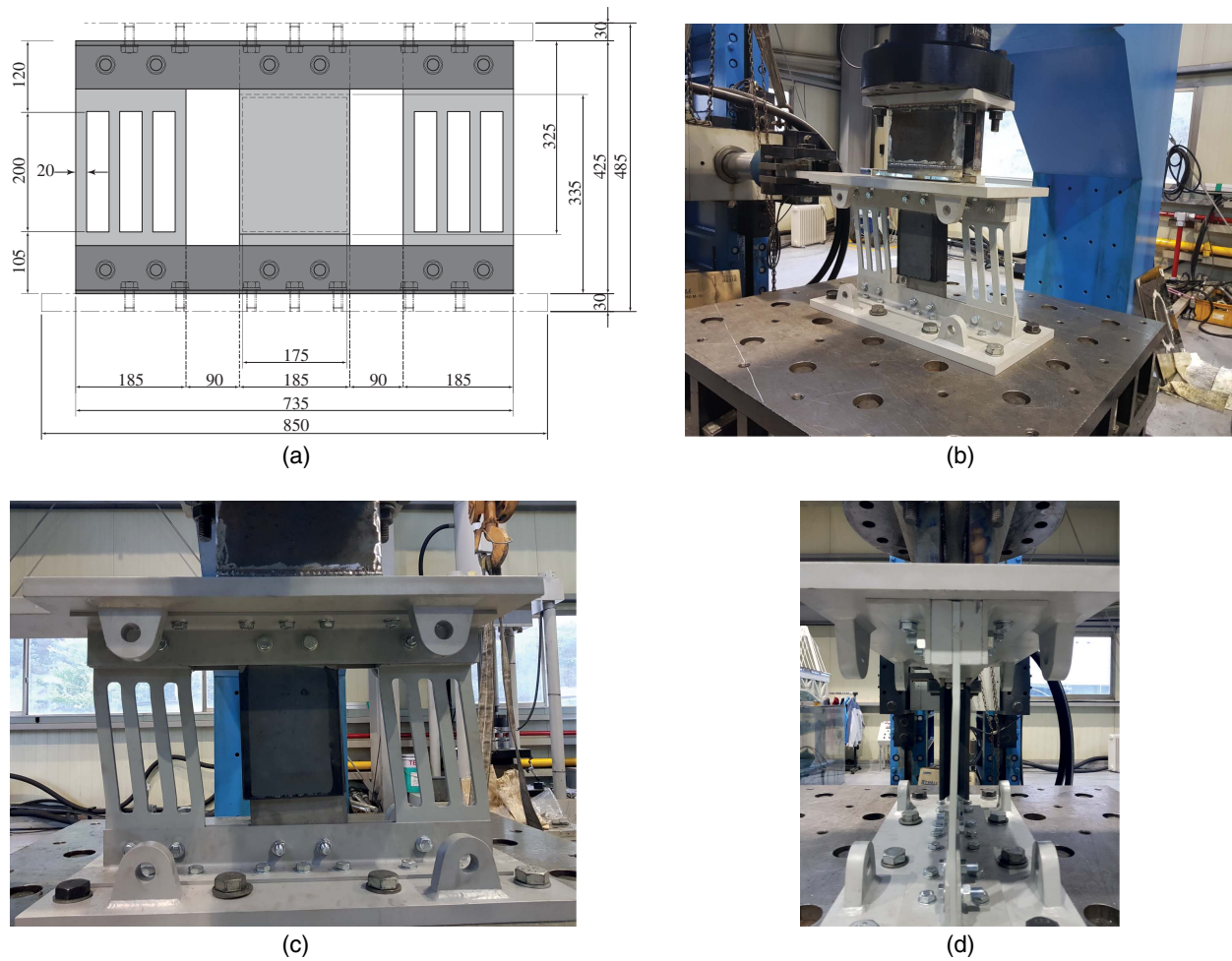


Fig. 6. Test of the HSVD: (a) dimensions of the test specimen; (b) test setup; (c) front view; and (d) side view.

of the 28th loading cycle, some of the strips in the slit damper fractured and the load was drastically decreased [Fig. 7(b)]. No significant damage was observed in the viscoelastic damper at this loading cycle. Fig. 7(c) depicts the hysteresis curves of the hybrid damper obtained from the test and the analysis model. To analyze the structure with the HSVDs, the BWBN model is implemented to represent the behavior of the viscoelastic part. Also, the material SteelMPF (Giuffrè–Menegotto–Pinto extended model) (Filippou et al. 1983) is applied to represent the nonlinear behavior of the steel slit part. SteelMPF is a modification of the bilinear model, and enables the model to make a smooth transition between the linear paths. In fact, SteelMPF utilized in OpenSees software is essentially the Giuffrè–Menegotto–Pinto model (Amini et al. 2018) with features for isotropic hardening. Based on the comparison, it is concluded that the use of the material SteelMPF and the modified BWBN model offers good agreement with the experimental results. For more information on material models and their parameters, the readers are referred to the OpenSees manual (McKenna et al. 2000).

Application to an Analysis Model Structure

Structural Details and Analysis Modeling

The SAC Phase II project developed three nonlinear buildings for the Los Angeles region to establish a transparent basis for evaluating different control devices [FEMA 355C (FEMA 2000b);

Ohtori et al. 2004]. They are approximate representations of typical low-rise, medium-rise, and high-rise buildings. In this study, the three-story moment-resisting frame is chosen from the SAC Phase II project to assess the effectiveness of the hybrid dampers. The structure was designed as a standard office building situated on stiff soil (soil type S2). The structural members were designed for wind and seismic loads as well as gravity loads per the Uniform Building Code (UBC 1994). The structural design and member properties of the aforementioned building can be found in detail in Ohtori et al. (2004) and Hossain et al. (2013).

Figs. 8(a and b) show the structural plan and the elevation view of the selected model building. The widths of all bays are 9.15 m and the floor-to-floor height of each story is 3.96 m. The yield strengths of the columns and the beams are 345 and 248 MPa, respectively. The perimeter beams have a fixed connection with the columns, whereas the interior beams have a hinged connection with the columns. The seismic mass of the first and the second floor including steel framing is 9.57×10^5 kg and that of the third floor is 1.04×10^6 kg. The fundamental natural period of the three-story frame is found to be 1.39 s.

The exterior moment frame in the short direction of the case study structure is taken as a two-dimensional (2D) analysis model considering the symmetry in the two principal directions. The simply supported beams and columns are modeled using the *elasticBeamColumn* elements in the OpenSees software, and are connected together by *zeroLength* elements with the negligible stiffness. The *beamWithHinges* element is used for modeling of

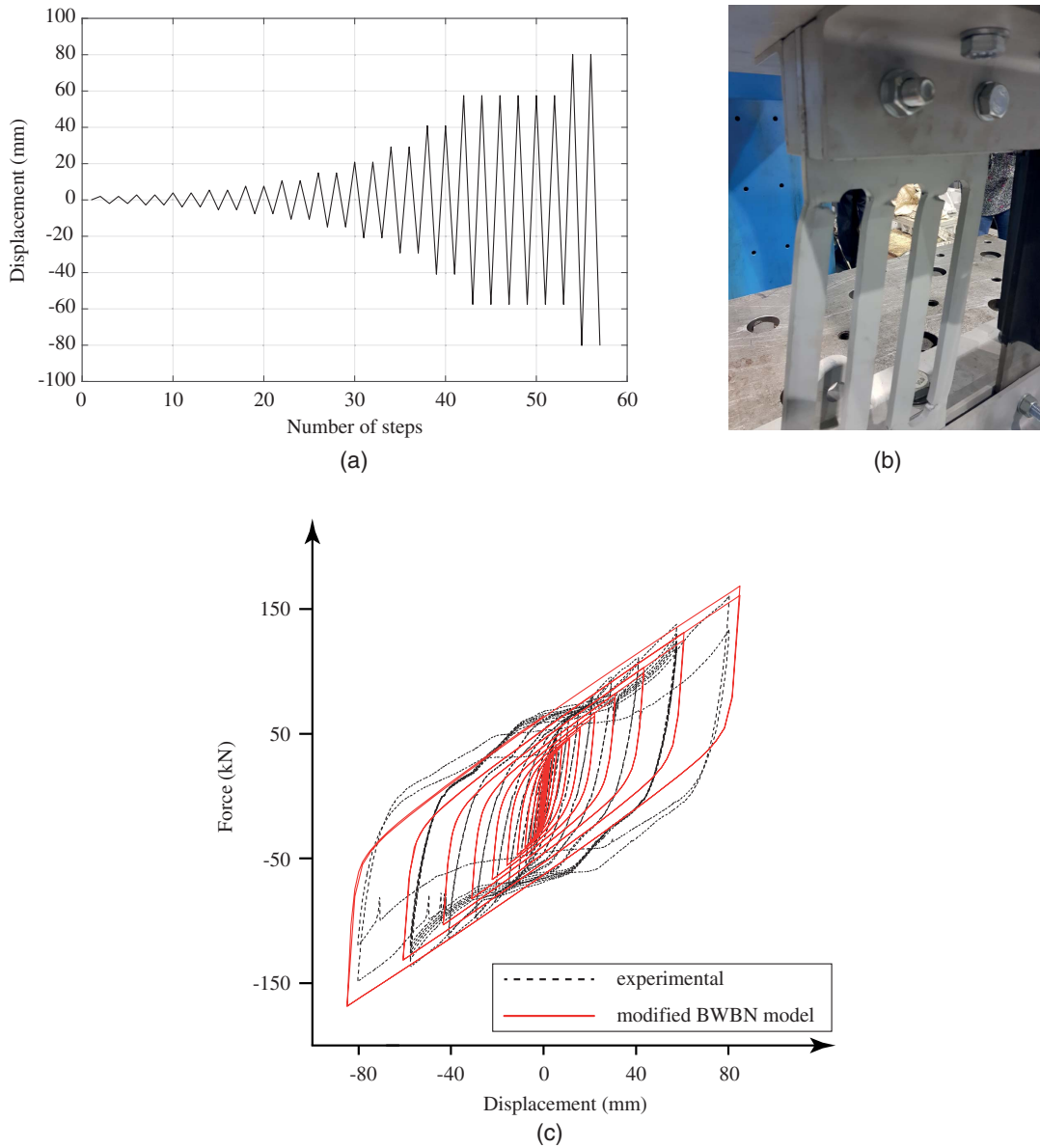


Fig. 7. Test results of the HSVD and the OpenSees simulation: (a) loading protocol; (b) fracture of slits; and (c) hysteresis curves.

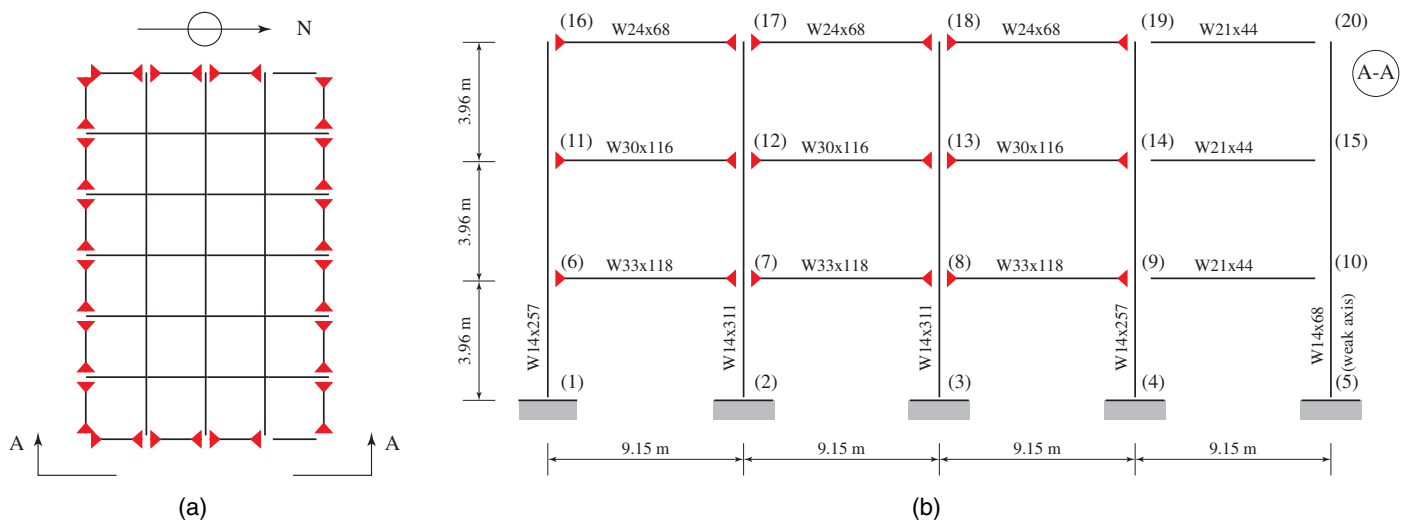


Fig. 8. Configuration of the three-story structure: (a) structural plan; and (b) elevation view.

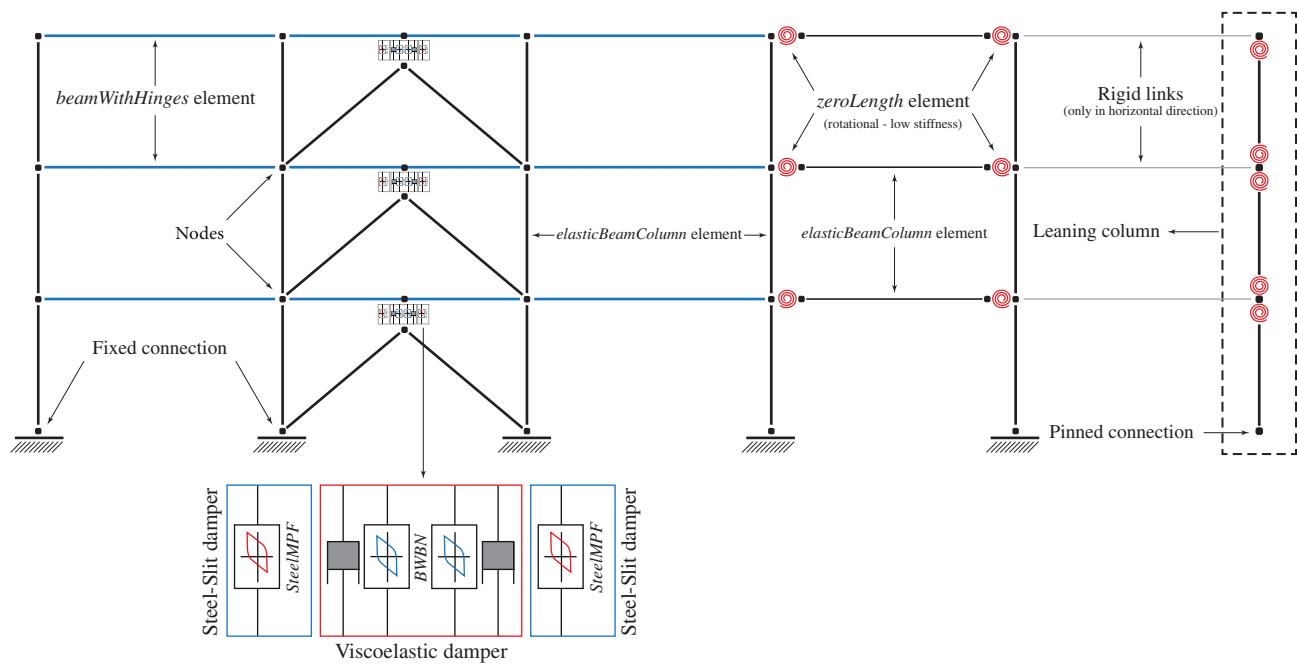


Fig. 9. OpenSees modeling of the three-story frame retrofitted with HSVDs.

the rigidly connected beams. The region of plastic hinges at both ends of them is assumed to be 10% of their lengths. The plastic hinges are modeled by fiber section and *Hardening* material, which is a combination of isotropic and linear kinematic hardening (McKenna et al. 2000). Rayleigh damping is applied to the first and the third modes of the structure with the damping ratio of 2% [FEMA 440 (FEMA 2005)]. To account for the P-Delta effect, a fictitious leaning column is connected by the rigid links to the three-story frame. The *elasticBeamColumn* element is implemented to model the fictitious leaning column connected to the rigid links by hinges, which are modeled by the *zeroLength* element with very small stiffness. The rigid links are assumed moment released at its ends, and work only as the translational constraints between the frame and the leaning frame. The structure is retrofitted by installing HSVDs at each story of the middle bay. Fig. 9 illustrates the schematic representation of the retrofitted three-story frame with HSVDs in the OpenSees platform. More details on modeling of the case study structure can be found in Hossain et al. (2013).

Ground Motions Selection

To evaluate the performance of the HSVD and its efficiency in comparison with the steel slit damper, 10 earthquake records are chosen

from the PEER NGA database (Ancheta et al. 2014), and are scaled to meet the design response spectrum of Los Angeles and the soil site is classified as stiff soil. Table 1 shows the 10 ground motion records. The design spectral response acceleration parameters are $SDS = 1.408g$ for short periods and $SD1 = 0.733g$ at the period of 1 s. Each ground motion record is scaled so that its square root of the sum of the squares (SRSS) spectrum does not fall below the design spectrum between the period range of $0.2T$ and $1.5T$ (ASCE 2013). The design spectrum at Los Angeles for the site class D and response spectrum of the scaled ground motion records are shown in Fig. 10. It is observed that the maximum interstory drift of the model structure obtained from nonlinear dynamic analysis ranges from 6% to 8% of the story height when subjected to the 10 ground motions, which is reduced to below 5% of the story height after seismic retrofit.

Evaluation of Performance Indices

In this section, seismic performance of the model structure is evaluated before and after seismic retrofit with the steel slit dampers and HSVDs based on various seismic performance indices. Ohtori et al. (2004) proposed a number of evaluation criteria to make comparison of different dampers. The evaluation criteria selected in this study are listed in Table 2. J_1 compares the maximum interstory

Table 1. Ground motion records used in the analysis

Ground motions	Station	Magnitude	Rupture distance (km)	PGA (g)	PGV (cm/s)	PGMD record number
Tabas, Iran	Tabas, 1978	7.35	2.1	0.825	99.21	143
Imperial Valley	Delta, 1979	6.53	22	0.239	26.88	169
Irpinia, Italy	Auletta, 1980	6.9	9.6	0.056	3.397	284
Superstition Hills	Brawley airport, 1987	6.54	17	0.155	10.74	719
Loma Prieta	San Francisco, 1989	6.93	63.1	0.0526	7.072	804
Landers	Mission Creek, 1992	7.28	27	0.124	6.743	880
Kocaeli, Turkey	Botas, 1999	7.51	127.1	0.108	9.21	1,153
Chi-Chi, Taiwan	TCU076, 1999	7.62	2.8	0.289	62.28	1,511
Hector Mine	Whitewater Trout Farm, 1999	7.13	62.9	0.056	5.076	1,838
Denali, Alaska	TAPS Pump, 2002	7.9	104.9	0.044	5.298	2,112

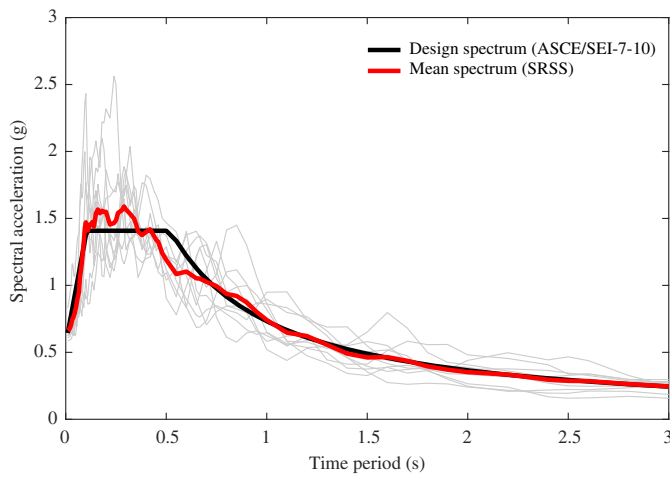


Fig. 10. Design spectrum and SRSS spectra of the earthquake ground motions used in the analysis.

Table 2. Performance criteria to be evaluated

Name	Summary	Formula
J_1	Interstory drift ratio	$\frac{\max_{t,i} \frac{ d_i(t) }{h_i}}{\delta_{\max}^{\text{max}}}$
J_2	Story acceleration	$\frac{\max_{t,i} \ddot{x}_{ai}(t) }{\ddot{x}_a^{\max}}$
J_3	Base shear	$\frac{\max_t \sum_i m_i \ddot{x}_{ai}(t) }{F_b^{\max}}$
J_4	Normed interstory drift ratio	$\frac{\max_{t,i} \frac{ d_i(t) }{h_i}}{\ \delta_{\max}^{\text{max}}\ }$
J_5	Normed level acceleration	$\frac{\max_{t,i} \ \ddot{x}_{ai}(t)\ }{\ \ddot{x}_a^{\max}\ }$
J_6	Normed base shear	$\frac{\ \sum_i m_i \ddot{x}_{ai}(t)\ }{\ F_b^{\max}\ }$

drift ratio of the bare structure and the structure retrofitted with the HSVDs and slit dampers; δ_{\max} is the maximum interstory drift ratio of the structure, h_i is the height of the corresponding floor, and $d_i(t)$ is the interstory drift ratio of the i th floor during an earthquake. J_2 is the acceleration ratio between the bare structure and the retrofitted

structure; \ddot{x}_a^{\max} is the absolute acceleration of the bare structure, and $\ddot{x}_{ai}(t)$ is the acceleration of the i th floor of the retrofitted structure. J_3 is the base shear ratio between the retrofitted structure and the bare structure; F_b^{\max} and m_i are defined as the maximum base shear of the structure and the mass of i th floor, respectively. The remaining evaluation criteria, J_4 , J_5 , and J_6 , are the normed values of maximum interstory drift ratios, absolute acceleration, and base shear, respectively. Eq. (18) gives the normed value of a time history response

$$\|\cdot\| = \sqrt{\frac{1}{t_f} \int_0^{t_f} (\cdot)^2 dt} \quad (18)$$

where t_f = time that is sufficient to attenuate structural responses.

The evaluation criteria averaged over all earthquakes used in the analysis are shown in Table 3 for eight earthquake peak ground accelerations (PGAs), varying from 0.3g to 1.0g. In addition to carrying out a comprehensive assessment, the mean values of each evaluation criterion for the eight PGAs are shown in the last column of Table 3. The most obvious finding from the values of Table 3 is that adding a viscoelastic damper considerably improves performance of the steel slit damper in decreasing lateral drift, acceleration, and base shear of the model structure. More specifically, the maximum interstory drift ratios of the structure, J_1 , decreased by 15% after adding a viscoelastic part. Furthermore, J_4 shows a 22% reduction in the normed interstory drift ratio. The HSVD is moderately successful in improving the performance of the steel slit dampers in reducing the maximum and normed acceleration levels. Both J_2 and J_5 , the maximum and the normed acceleration levels, were decreased by 3.2%, respectively. The base shear plays a significant role in the design of low-rise structures subjected to seismic load, and the HSVDs improved performance of the steel slit dampers in reducing the maximum and the normed base shear, J_3 and J_6 , by 5.5% and 7.7%, respectively. The reason for the relatively moderate improvement of the hybrid dampers over the slit dampers is that the shear area of the viscoelastic damper used in this study is much smaller than that of a commercially available one. It was made so small to be fitted to the dynamic fatigue tester. It is observed that the fundamental natural period of the structure decreased from 1.38 to 1.23 s after seismic retrofit using the hybrid dampers. This implies that the added dampers contribute only minutely to the increase in stiffness. The contribution of the damper is expected to increase once the damper with a more realistic size is used for seismic retrofit.

Table 3. Evaluated performance indices

Criteria	Dampers	Earthquake intensity								Mean
		0.3g	0.4g	0.5g	0.6g	0.7g	0.8g	0.9g	1.0g	
J_1	HSVD	0.882	0.884	0.901	0.903	0.893	0.893	0.911	0.921	0.898
	Slit	0.924	0.927	0.949	0.949	0.941	0.953	0.964	0.965	0.947
J_2	HSVD	0.893	0.920	0.911	0.920	0.942	0.957	0.932	0.954	0.928
	Slit	0.904	0.920	0.916	0.946	0.977	0.970	0.947	0.987	0.946
J_3	HSVD	0.920	0.926	0.939	0.958	0.978	0.991	0.995	0.972	0.960
	Slit	0.932	0.940	0.956	0.969	0.980	0.986	0.984	0.976	0.965
J_4	HSVD	0.839	0.878	0.888	0.890	0.897	0.900	0.904	0.908	0.888
	Slit	0.880	0.919	0.929	0.937	0.942	0.949	0.953	0.956	0.933
J_5	HSVD	0.835	0.866	0.889	0.907	0.919	0.929	0.931	0.932	0.901
	Slit	0.834	0.870	0.888	0.909	0.928	0.936	0.939	0.942	0.906
J_6	HSVD	0.845	0.870	0.895	0.913	0.925	0.935	0.942	0.948	0.909
	Slit	0.846	0.874	0.899	0.915	0.928	0.937	0.943	0.948	0.911

Fragility Analysis

Seismic fragility can be defined as the probability of a structural component or a system to fail to perform satisfactorily under a pre-defined seismic action. Fragility curves can be developed for structural and nonstructural components and structural systems. In this study, the damage states in the individual elements are neglected and seismic fragility of the model structure is estimated in the system level only based on the maximum interstory drift as recommended in FEMA 356 (FEMA 2000a). To obtain the statistical distribution of the dynamic response, fragility analyses are conducted on the model structure before and after implementing the HSVDs and only slit dampers. Based on the dynamic analysis results of the 10 earthquakes used previously, the probability of reaching the limit states, which are immediate occupancy (IO), life safety (LS), and collapse prevention (CP), are obtained for the analysis model. The fragility function can be defined by Eq. (19) as a lognormal cumulative distribution function indicating the probability of collapse at the limit states (Porter et al. 2007)

$$P(C|IM = x) = \Phi\left(\ln\left(\frac{x}{\theta}\right) / \beta\right) \quad (19)$$

where $P(C|IM = x)$ = probability that an earthquake with an intensity measure $IM = x$ leads to the collapse of a structure. Φ is the standard normal cumulative distribution in which θ and β are the median value of the fragility function and standard deviation of $\ln(IM)$, respectively. In this study, the maximum interstory drift ratios of 1.0%, 2.5%, and 5% are assumed to be the IO, LS, and CP limit states, respectively, and the seismic fragility is estimated based on the maximum interstory drift. In the consideration of these drift limit states, the failure or damage in dampers is not considered based on the assumption that they can be manufactured in such a

way that the deformability of the dampers satisfies the displacement demand by controlling the size of each component of the dampers.

The fragility curves corresponding to the limit states of the model structure are presented in Fig. 11 before and after seismic retrofit. Fig. 11 demonstrates that, as expected, the retrofitted frame with HSVDs (viscoelastic + slit dampers) has the smallest probability of collapse at all seismic intensity in comparison with the bare frame and the frame retrofitted with slit dampers. It can be concluded that adding viscoelastic dampers in parallel with the slit dampers improves the performance of the structure rather significantly. According to Fig. 11, the HSVDs decreased the probability of collapse of bare frame by up to 45%, 26%, and 20% in the IO, LS, and CP limit states, respectively. It is also observed that the viscoelastic part improved the performance of the slit dampers in reducing probability of collapse by 17%, 12.5%, and 12% in the IO, LS, and CP limit states, respectively. This shows that the addition of the viscoelastic dampers is more effective in the IO limit state than in the LS and CP states. The result seems to be reasonable considering that, in the relatively small displacement under minor earthquakes, the steel slit dampers behave elastically or experience small inelastic deformation with only small energy dissipation.

Design Procedure and Application

In this section, another case study building is selected to present a design procedure for the dampers to meet a given target performance. The selected structure is a four-story steel office building assumed to be located on site class D soil in downtown Los Angeles. The building is designed in accordance with AISC (2010a, b). The risk category of the building is II and its importance factor is 1.0. The lateral force-resisting system of this building is the special moment frame (SMF) at perimeters designed with reduced beam section (RBS) connections as per AISC (2010b). The gravity columns and beams are designed with $W14 \times 90$ and $W24 \times 55$, respectively. In addition,

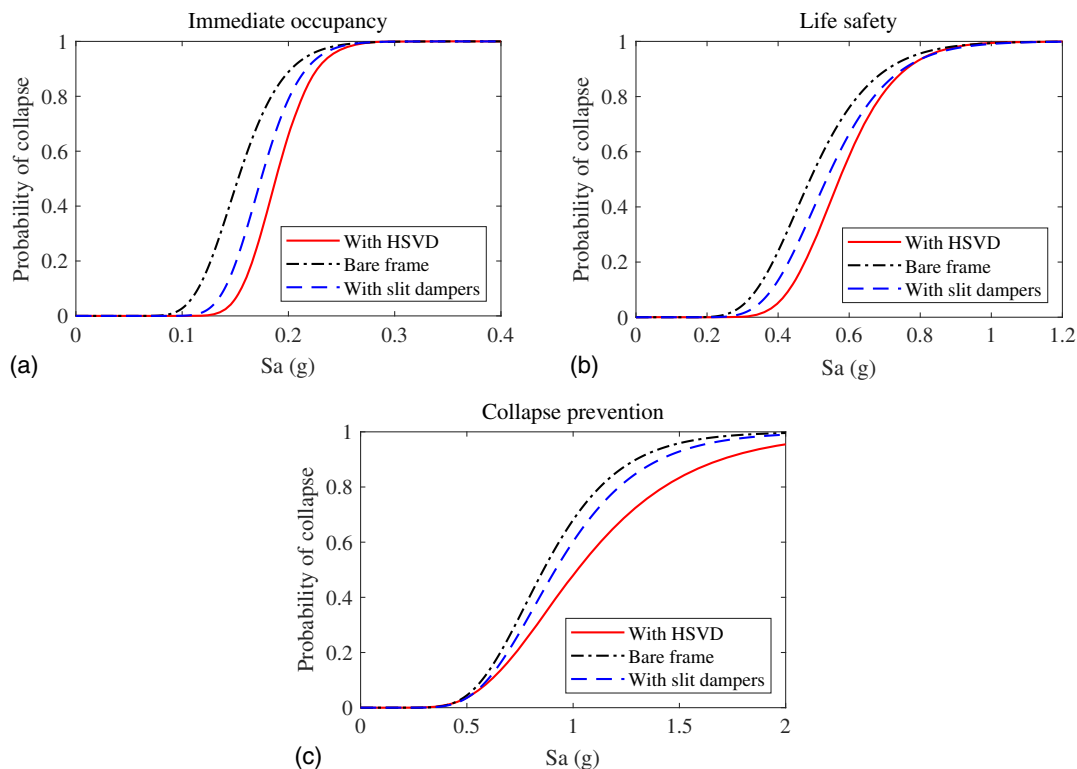


Fig. 11. Fragility curves corresponding to the IO, LS, and CP limit states of the model structure before and after seismic retrofit.

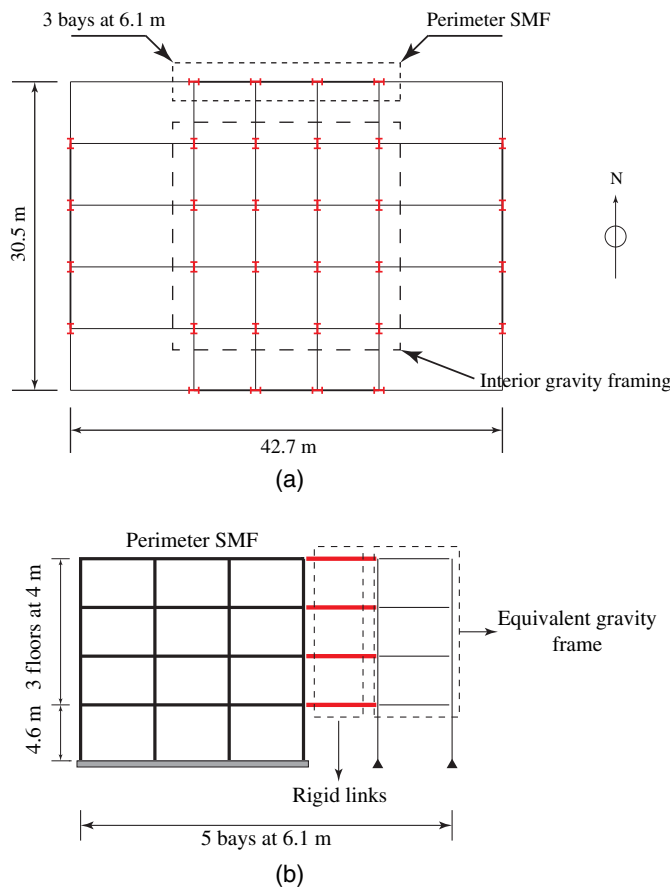


Fig. 12. Configuration of the four-story case study structure: (a) structural plan; and (b) elevation.

the interior gravity frames are designed as typical single-plate shear-tab beam-to-column connections. Fig. 12 shows the structural plan and elevation of the four-story building. In this study, the SMF in the East–West (EW) direction is selected as a prototype frame to evaluate seismic performance of the HSVD. More details on the design and properties of the building can be found in Lignos and Krawinkler (2011). The prototype frame is modeled analytically using the OpenSees software, similarly to the previous case study structure.

According to preliminary analysis of the case study structure, the maximum interstory drift is found to be larger than the limit state of 2% of the story height and thus seismic retrofit is required. To obtain the required damping to meet this limit state, the capacity and the demand diagram technique provided in ATC40 is implemented. To this end, the demand curve (response spectrum) and the capacity curve (pushover curve) are plotted in the spectral acceleration versus spectral displacement format as shown in Fig. 13. The fundamental mode shape is considered to obtain the pushover curve, which is idealized as a bilinear curve and is transferred into the spectral acceleration versus spectral displacement domain. The 5% elastic demand spectrum for the maximum considered event level is also transferred into the same domain. For seismic retrofit, the target maximum interstory drift ratio is set to be 2.0%, which is 0.254 m in the equivalent single degree of freedom system. Using this target displacement as a cross point of the demand and the capacity curves, the required effective damping ratio of 44.5% is obtained from the diagram. The amount of the hybrid dampers required to meet the extra effective damping is determined based on the ASCE 41-13 formula

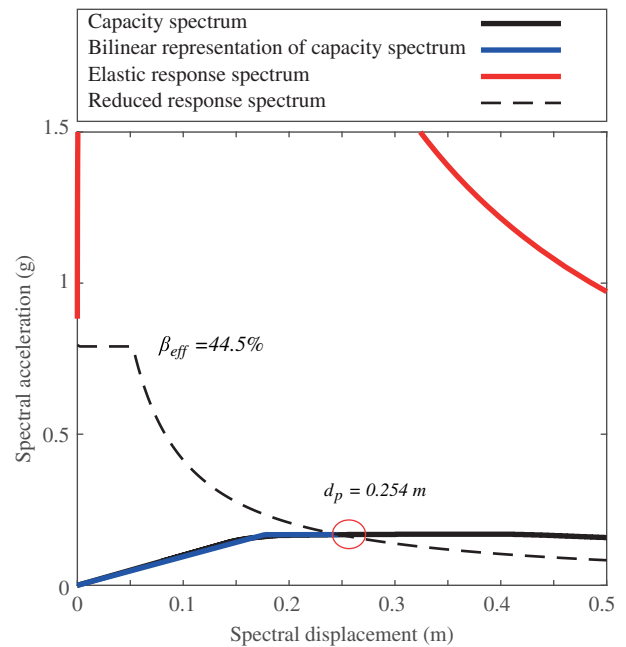


Fig. 13. Estimation of the required damping in a spectral acceleration versus spectral displacement domain.

$$\beta_{\text{eff}} = \frac{\sum_j W_j}{4\pi W_k} \quad (20)$$

where W_j = work by linear viscous device j in one complete loading cycle; and W_k = maximum strain energy in the structure. Even though many different combinations of viscoelastic pad and slit dampers are possible, the viscoelastic pad size of 7,310 cm² and 72 slits per story are used in this study. They are divided into three separate hybrid dampers, one for each bay.

Fig. 14 shows the roof displacement time histories of the model structure before and after seismic retrofit subjected to the RSN143-Tabas and RSN719-Superstition Hills earthquakes. It can be observed that after seismic retrofit, the maximum and the residual displacements of the structure decrease significantly. Fig. 15 depicts the maximum interstory drifts of the model structure subjected to the seven scaled earthquakes, where it can be observed that the interstory drifts are decreased within the target value of 2% of the story height after seismic retrofit using the hybrid dampers. Fig. 16 shows the cumulative energy dissipated by the dampers when the structure is subjected to the RSN143-Tabas and RSN719-Superstition Hills earthquakes. It can be noticed that a significant amount of seismic input energy is effectively dissipated by the dampers. It is observed that the fundamental natural period of the structure decreased from 1.55 to 0.90 s after seismic retrofit. This implies that the added dampers contribute significantly to the increase in stiffness. Therefore, the reduction in seismic response of the model structure after seismic retrofit may be contributed from both the increase in stiffness and energy dissipation capacity of the added dampers.

Conclusions

In this study, a HSVD was developed by combining steel slit and viscoelastic dampers connected in parallel to enhance the seismic performance of structures. Cyclic loading tests were conducted for both the viscoelastic damper and the hybrid damper to validate the

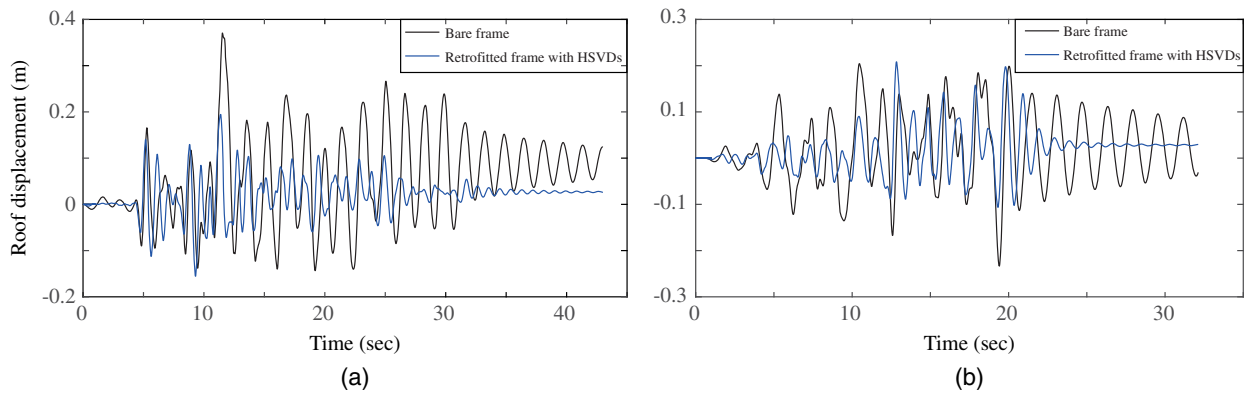


Fig. 14. Roof displacement time histories of the model structure before and after seismic retrofit: (a) RSN143-Tabas earthquake; and (b) RSN719-Superstition Hills earthquake.

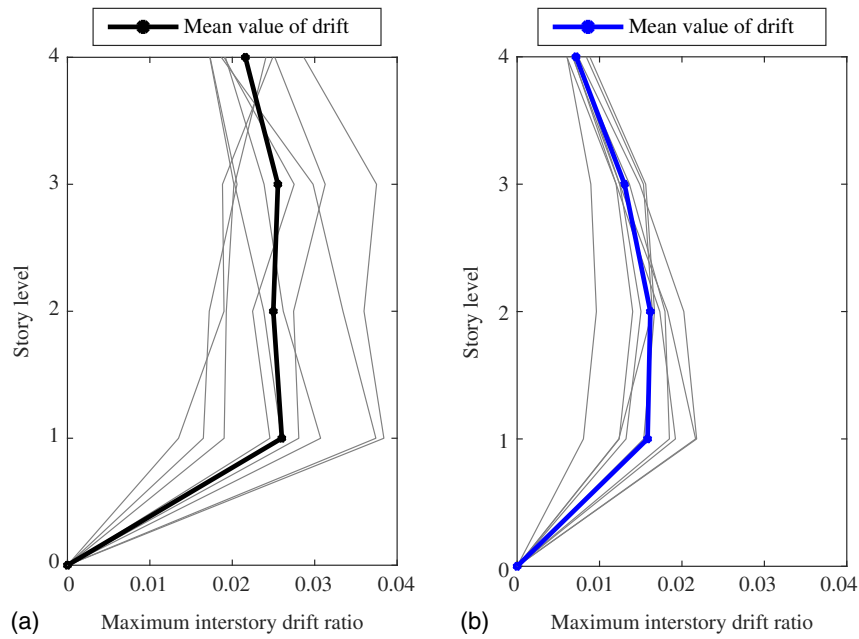


Fig. 15. Maximum interstory drifts of the model structure subjected to the seven scaled earthquakes: (a) before seismic retrofit; and (b) after seismic retrofit.

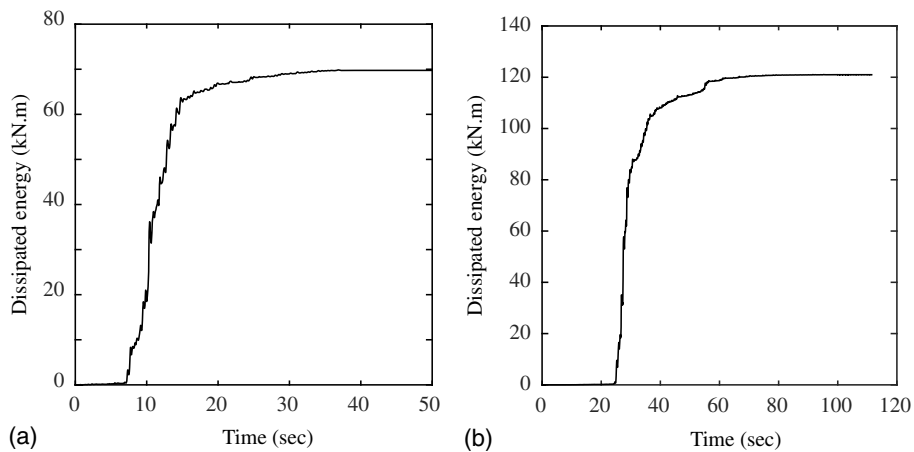


Fig. 16. Cumulative energy dissipated by the dampers: (a) RSN143-Tabas earthquake; and (b) RSN719-Superstition Hills earthquake.

energy dissipation capability and the analysis model developed using the nonlinear BWBN model. A three-story moment-resisting frame was chosen from the SAC Phase II project, and the analytical model was used to assess the effectiveness of the HSVDs for seismic retrofit. In order to gain an insight into the performance of the hybrid dampers, six performance criteria were used to compare the responses of the structure before and after seismic retrofit with the steel slit dampers and HSVDs. Fragility analysis was then carried out to investigate the exceedance probability of specified limit states. Finally, a capacity and demand diagram approach was applied to estimate the required equivalent damping for seismic retrofit to meet a given target performance point.

The analysis results of the structure retrofitted using HSVDs showed that adding viscoelastic dampers in parallel with the steel slit dampers improved the performance of the steel slit dampers significantly. It was also observed that the proposed BWBN model turned out to be in better agreement with the experimental results than the conventional Kelvin–Voigt model. The fragility analysis showed that, after seismic retrofit with the HSVDs, the probabilities of reaching the damage states were reduced, especially in the IO limit state. It was also observed that the HSVDs could be more effective for small-to-medium earthquakes. Finally, the use of the capacity and demand diagram procedure turned out to be effective in preliminary design of the hybrid dampers to meet a desired target performance point. Because the small-scale viscoelastic dampers used in this study are less expensive to manufacture than the full-scale one currently available in the seismic retrofit market, and because the steel slit dampers are a cost-effective device, especially for large earthquakes, the hybrid dampers may be applied as efficient seismic energy dissipation devices effective both for small and large earthquakes. However, the paper is limited by the fact that only simplified seismic fragility analysis was carried out based on interstory drift of the model structure. More detailed seismic fragility can be evaluated by considering damage states at the element level. Also, for practical application of the damper, temperature dependency of the viscoelastic material in the hybrid damper needs to be quantified through a series of tests and applied in the design.

Data Availability Statement

Some or all data, models, or code generated or used during the study are available from the corresponding author by request.

Acknowledgments

This research was carried out by Land Transport Technology Promotion Research Project (task No. 19CTAP-C153076-01) of the Ministry of Land, Infrastructure and Transport.

References

- AISC. 2010a. *Prequalified connections for special and intermediate steel moment frames for seismic applications*. ANSI/AISC 358-10. Chicago: AISC.
- AISC. 2010b. *Seismic provisions for structural steel buildings*. ANSI/AISC 341-10. Chicago: AISC.
- Amini, F., M. Bitaraf, M. S. Eskandari, and M. M. Javidan. 2018. "Impacts of soil-structure interaction on the structural control of nonlinear systems using adaptive control approach." *Eng. Struct.* 157 (Feb): 1–13. <https://doi.org/10.1016/j.engstruct.2017.11.071>.
- Ancheta, T. D., et al. 2014. "NGA-West2 database." *Earthquake Spectra* 30 (3): 989–1005. <https://doi.org/10.1193/1070913EQS197M>.
- ASCE. 2013. *Seismic evaluation and retrofit of existing buildings*. ASCE 41. Reston, VA: ASCE.
- Chan, R. W. K., and F. Albermani. 2008. "Experimental study of steel slit damper for passive energy dissipation." *Eng. Struct.* 30 (4): 1058–1066. <https://doi.org/10.1016/j.engstruct.2007.07.005>.
- FEMA. 1997. *NEHRP guidelines for the seismic rehabilitation of buildings*. FEMA 273. Washington, DC: FEMA.
- FEMA. 2000a. *Prestandard and commentary for the seismic rehabilitation of buildings*. FEMA 356. Washington, DC: FEMA.
- FEMA. 2000b. *State of the art report on systems performance of steel moment frames subject to earthquake ground shaking*. FEMA 355C. Washington, DC: FEMA.
- FEMA. 2005. *Improvement of nonlinear static seismic analysis procedures*. FEMA 440. Washington, DC: FEMA.
- FEMA. 2007. *Interim testing protocols for determining the seismic performance characteristics of structural and nonstructural components*. FEMA 461. Washington, DC: FEMA.
- Filippou, F. C., E. P. Popov, and V. V. Bertero. 1983. "Modeling of R/C joints under cyclic excitations." *J. Struct. Eng.* 109 (11): 2666–2684. [https://doi.org/10.1061/\(ASCE\)0733-9445\(1983\)109:11\(2666\)](https://doi.org/10.1061/(ASCE)0733-9445(1983)109:11(2666)).
- Foliente, G. C. 1995. "Hysteresis modeling of wood joints and structural systems." *J. Struct. Eng.* 121 (6): 1013–1022. [https://doi.org/10.1061/\(ASCE\)0733-9445\(1995\)121:6\(1013\)](https://doi.org/10.1061/(ASCE)0733-9445(1995)121:6(1013)).
- Guo, J. W. W., and C. Christopoulos. 2016. "Response prediction, experimental characterization and P-spectra design of frames with viscoelastic-plastic dampers." *Earthquake Eng. Struct. Dyn.* 45 (11): 1855–1874. <https://doi.org/10.1002/eqe.2732>.
- Hossain, M. R., and M. Ashraf. 2012. "Mathematical modelling of yielding shear panel device." *Thin-Walled Struct.* 59 (Oct): 153161. <https://doi.org/10.1016/j.tws.2012.04.018>.
- Hossain, M. R., M. Ashraf, and J. E. Padgett. 2013. "Risk-based seismic performance assessment of yielding shear panel device." *Eng. Struct.* 56 (Nov): 1570–1579. <https://doi.org/10.1016/j.engstruct.2013.07.032>.
- Javidan, M. M., and J. Kim. 2019. "Seismic retrofit of soft-first-story structures using rotational friction dampers." *J. Struct. Eng.* 145 (12): 04019162. [https://doi.org/10.1061/\(ASCE\)ST.1943-541X.0002433](https://doi.org/10.1061/(ASCE)ST.1943-541X.0002433).
- Javidan, M. M., and J. Kim. 2020. "Experimental and numerical sensitivity assessment of viscoelasticity for polymer composite materials." *Sci. Rep.* 10 (1): 675. <https://doi.org/10.1038/s41598-020-57552-3>.
- Kasai, K., M. Teramoto, and Y. Watanabe. 2002. "Behavior of a passive control damper combining visco-elastic and elasto-plastic devices in series." *Trans. AIJ* 67 (556): 51–58. https://doi.org/10.3130/aajs.67.51_1.
- Kim, J., and H. Shin. 2017. "Seismic loss assessment of a structure retrofitted with slit-friction hybrid dampers." *Eng. Struct.* 130 (Jan): 336–350. <https://doi.org/10.1016/j.engstruct.2016.10.052>.
- Lee, C. H., J. Kim, D. H. Kim, J. Ryu, and Y. K. Ju. 2016. "Numerical and experimental analysis of combined behavior of shear-type friction damper and non-uniform strip damper for multi-level seismic protection." *Eng. Struct.* 114 (May): 75–92. <https://doi.org/10.1016/j.engstruct.2016.02.007>.
- Lee, J., and J. Kim. 2015. "Seismic performance evaluation of moment frames with slit-friction hybrid dampers." *Earthquakes Struct.* 9 (6): 1291–1311. <https://doi.org/10.12989/eas.2015.9.6.1291>.
- Lee, J., and J. Kim. 2017. "Development of steel box-shaped slit dampers for seismic retrofit of building structures." *Eng. Struct.* 150 (Nov): 934–946. <https://doi.org/10.1016/j.engstruct.2017.07.082>.
- Lignos, D. G., and H. Krawinkler. 2011. "Deterioration modeling of steel components in support of collapse prediction of steel moment frames under earthquake loading." *J. Struct. Eng.* 137 (11): 1291–1302. [https://doi.org/10.1061/\(ASCE\)ST.1943-541X.0000376](https://doi.org/10.1061/(ASCE)ST.1943-541X.0000376).
- Marko, J., D. Thambiratnam, and N. Perera. 2004. "Influence of damping systems on building structures subject to seismic effect." *Eng. Struct.* 26 (13): 1939–1956. <https://doi.org/10.1016/j.engstruct.2004.07.008>.
- Marshall, J. D., and F. A. Charney. 2012. "Seismic response of steel frame structures with hybrid passive control systems." *Earthquake Eng. Struct. Dyn.* 41 (4): 715–733. <https://doi.org/10.1002/eqe.1153>.
- McKenna, F., G. Fenves, and S. Scott. 2000. *Open system for earthquake engineering simulation*. Berkeley, CA: Univ. of California.
- Montgomery, M., and C. Christopoulos. 2015. "Experimental validation of viscoelastic coupling dampers for enhanced dynamic performance of

- high-rise buildings." *J. Struct. Eng.* 141 (5): 04014145. [https://doi.org/10.1061/\(ASCE\)ST.1943-541X.0001092](https://doi.org/10.1061/(ASCE)ST.1943-541X.0001092).
- Naeem, A., M. N. Eldin, J. Kim, and J. Kim. 2017. "Seismic performance evaluation of a structure retrofitted using steel slit dampers with shape memory alloy bars." *Int. J. Steel Struct.* 17 (4): 1627–1638. <https://doi.org/10.1007/s13296-017-1227-4>.
- Naeem, A., and J. Kim. 2018a. "Seismic performance evaluation of a spring viscous damper cable system." *Eng. Struct.* 176 (Dec): 455–467. <https://doi.org/10.1016/j.engstruct.2018.09.055>.
- Naeem, A., and J. Kim. 2018b. "Seismic retrofit of a framed structure using damped cable systems." *Steel Compos. Struct.* 29 (3): 287–299. <https://doi.org/10.12989/scs.2018.29.3.287>.
- Nour Eldin, M., J. Kim, and J. Kim. 2018. "Optimal distribution of steel slit-friction hybrid dampers based on life cycle cost." *Steel Compos. Struct.* 27 (5): 633–646. <https://doi.org/10.12989/scs.2018.27.5.633>.
- Ohtori, Y., R. E. Christenson, B. F. Spencer, Jr., and S. J. Dyke. 2004. "Benchmark control problems for seismically excited nonlinear building." *J. Eng. Mech.* 130 (4): 366–385. [https://doi.org/10.1061/\(ASCE\)0733-9399\(2004\)130:4\(366\)](https://doi.org/10.1061/(ASCE)0733-9399(2004)130:4(366)).
- Pant, D. R., M. Montgomery, and C. Christopoulos. 2017. "Analytical study on the dynamic properties of viscoelastically coupled shear walls in high-rise buildings." *J. Eng. Mech.* 143 (8): 04017047. [https://doi.org/10.1061/\(ASCE\)EM.1943-7889.0001247](https://doi.org/10.1061/(ASCE)EM.1943-7889.0001247).
- Porter, K., R. Kennedy, and R. Bachman. 2007. "Creating fragility functions for performance-based earthquake engineering." *Earthquake Spectra* 23 (2): 471–489. <https://doi.org/10.1193/1.2720892>.
- Tsai, C., K. Chen, and C. Chen. 1998. "Seismic resistibility of high-rise buildings with combined velocity-dependent and velocity-independent devices." In Vol. 366 of *Proc., ASME Pressure Vessels and Piping Conf.*, 103–108. New York: ASME.
- UBC (Uniform Building Code). 1994. *Structural engineering design provisions*. Whittier, CA: International Conference of Building Officials.
- Uetani, K., M. Tsuji, and I. Takewaki. 2003. "Application of an optimum design method to practical building frames with viscous dampers and hysteretic dampers." *Eng. Struct.* 25 (5): 579–592. [https://doi.org/10.1016/S0141-0296\(02\)00168-2](https://doi.org/10.1016/S0141-0296(02)00168-2).
- Xiang, N., and M. S. Alam. 2019. "Comparative seismic fragility assessment of an existing isolated continuous bridge retrofitted with different energy dissipation devices." *J. Bridge Eng.* 24 (8): 04019070. [https://doi.org/10.1061/\(ASCE\)BE.1943-5592.0001425](https://doi.org/10.1061/(ASCE)BE.1943-5592.0001425).
- Xu, Z. D., Y. X. Liao, T. Ge, and C. Xu. 2016. "Experimental and theoretical study on viscoelastic dampers with different matrix rubbers." *J. Eng. Mech.* 142 (8): 04016051. [https://doi.org/10.1061/\(ASCE\)EM.1943-7889.0001101](https://doi.org/10.1061/(ASCE)EM.1943-7889.0001101).
- Xue, C. 2013. *Mechanical properties study for sandwich plate system*. Harbin, China: Harbin Engineering Univ.